Supplementary Information

Supplementary Figures

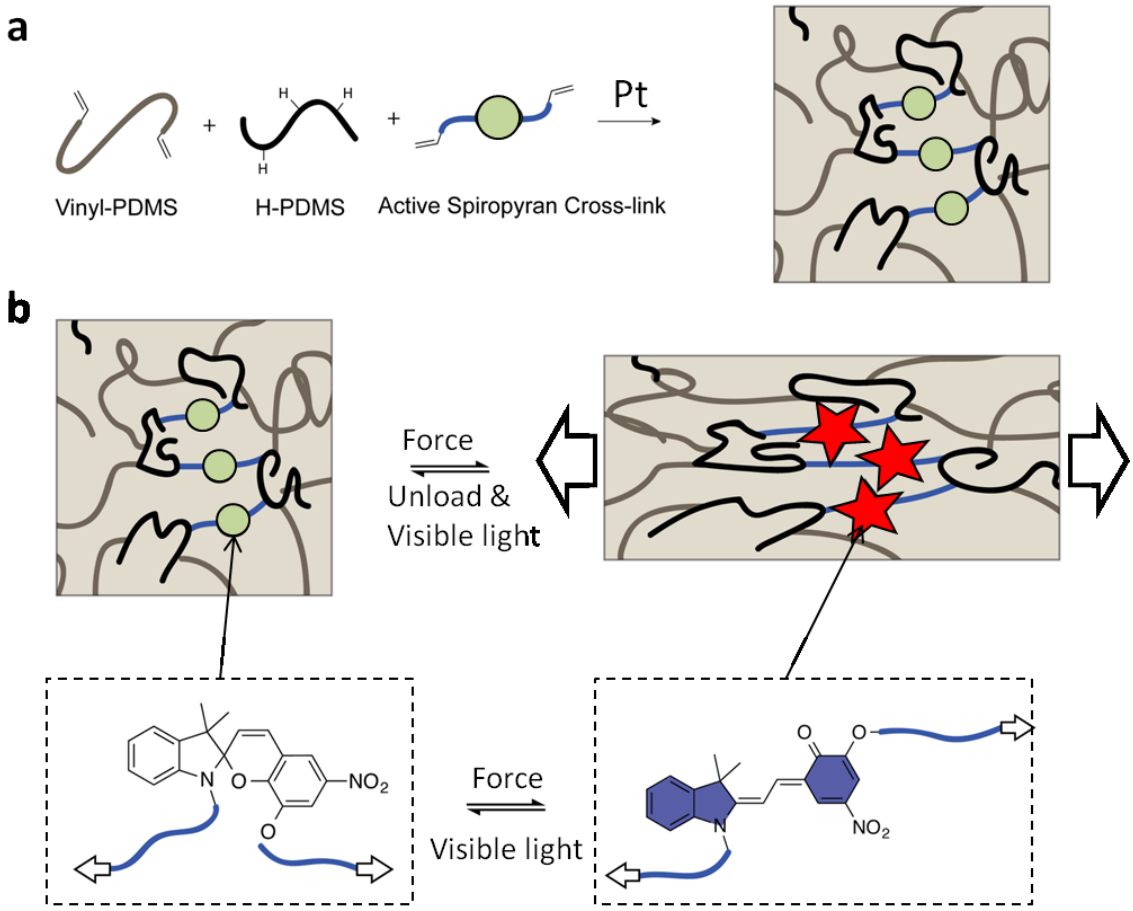

Supplementary Figure 1 | Covalently incorporating spiropyran into the Sylgard network. (a) A covalently crosslinked EMCR Sylgard network generated by combining Vinyl terminated PDMS, hydrosilylated PDMS and the bis-alkene functionalized spiropyran (as crosslinker) through a platinum-catalyzed hydrosilylation reaction. (b) Transition from the nearly colorless spiropyran to the colored merocyanine by a force-activated 6-π electrocyclic ring-opening reaction. Removing the deformation applied to the EMCR allows for thermal ring closure to the spiropyran form within ~ 10 min, or within 3 min upon illumination with a visible light (e.g., green light).

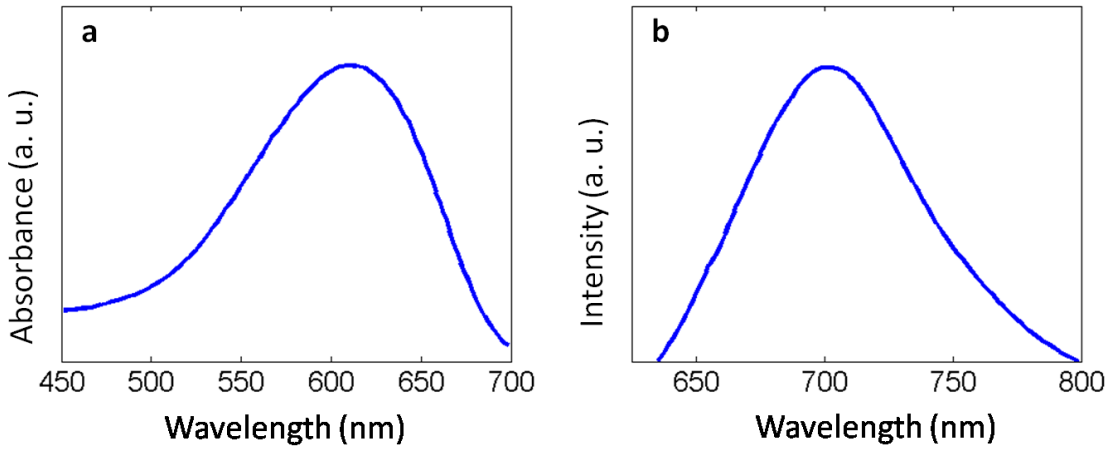

Supplementary Figure 2 | (a) Absorption and (b) emission spectra of the stress-activated merocyanine within the EMCR elastomer.

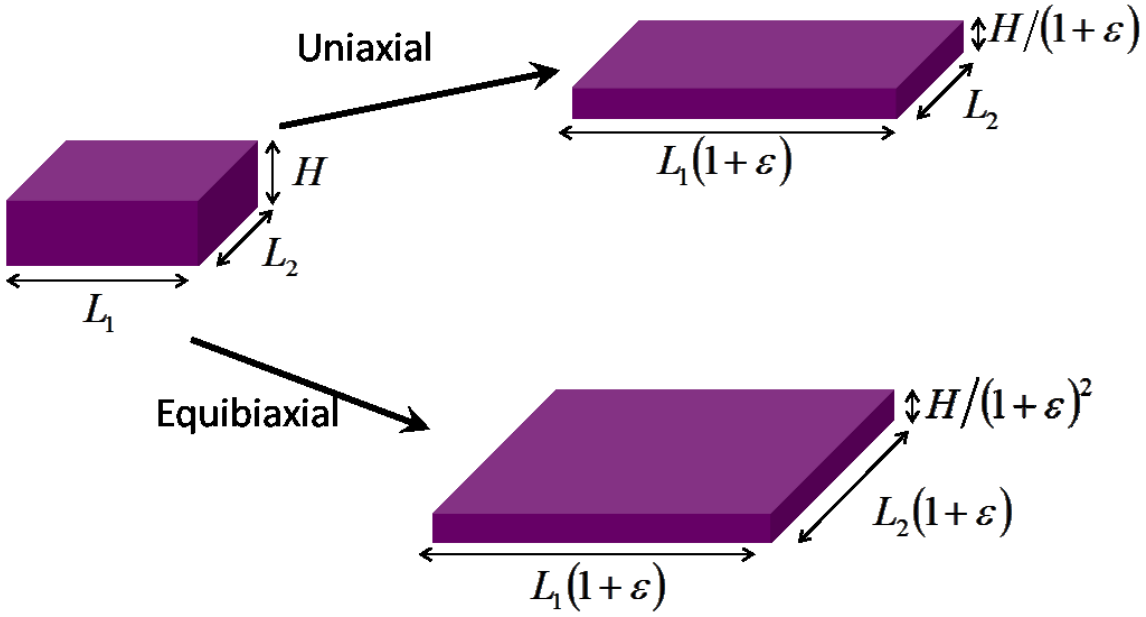

Supplementary Figure 3 | Schematic illustrations of uniaxial and equibiaxial deformation of the EMCR elastomers. The stretches (L/L_0) in three directions of the uniaxially deformed elastomer are $1+\varepsilon$, 1 and $1/(1+\varepsilon)$; therefore, the first invariant is calculated as $I=(1+\varepsilon)^2+1+(1+\varepsilon)^{-2}$. The stretches in three directions of the equibiaxially deformed elastomer are $\varepsilon+1$, $\varepsilon+1$ and $(\varepsilon+1)^{-2}$; therefore, the first invariant is calculated as $I=2(1+\varepsilon)^2+(1+\varepsilon)^{-4}$.

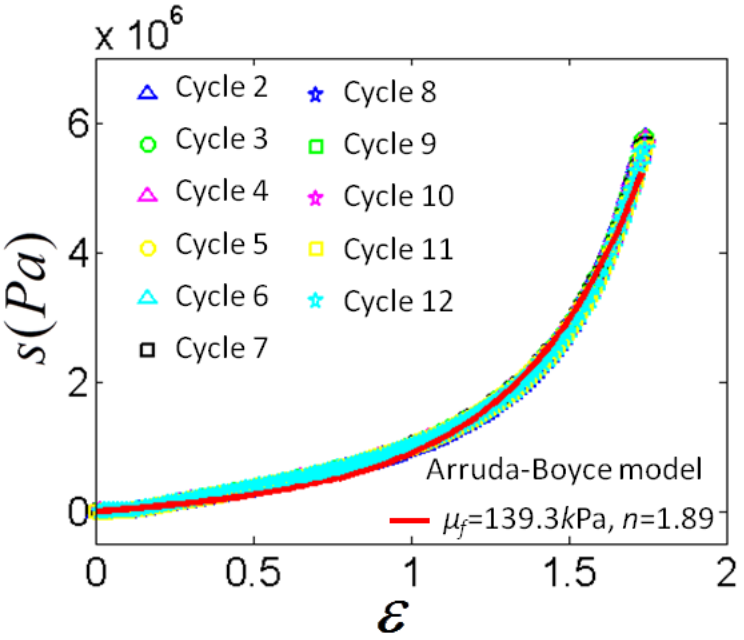

Supplementary Figure 4 | The nominal stress *vs.* strain curve of the EMCR Sylgard elastomer. The EMCR elastomer shows negligible hysteresis for more than 11 cycles after the first strain loading cycle. The nominal stress-strain curves are fitted to the Arruda-Boyce model, $s=\mu_f\left(\lambda-\lambda^{-2}\right)\left(1+\frac{I}{5n}+\frac{11I}{175n^2}+...\right)$, where s is the uniaxial nominal stress, $\lambda=1+\varepsilon$ is the stretch, $I=\lambda^2+2\lambda^{-2}$ is the first invariant, and n is a parameter that accounts for the stiffening effect. The fitted shear modulus of the EMCR elastomer is $\mu_f=139.3kPa$, and the fitted n is 1.89.

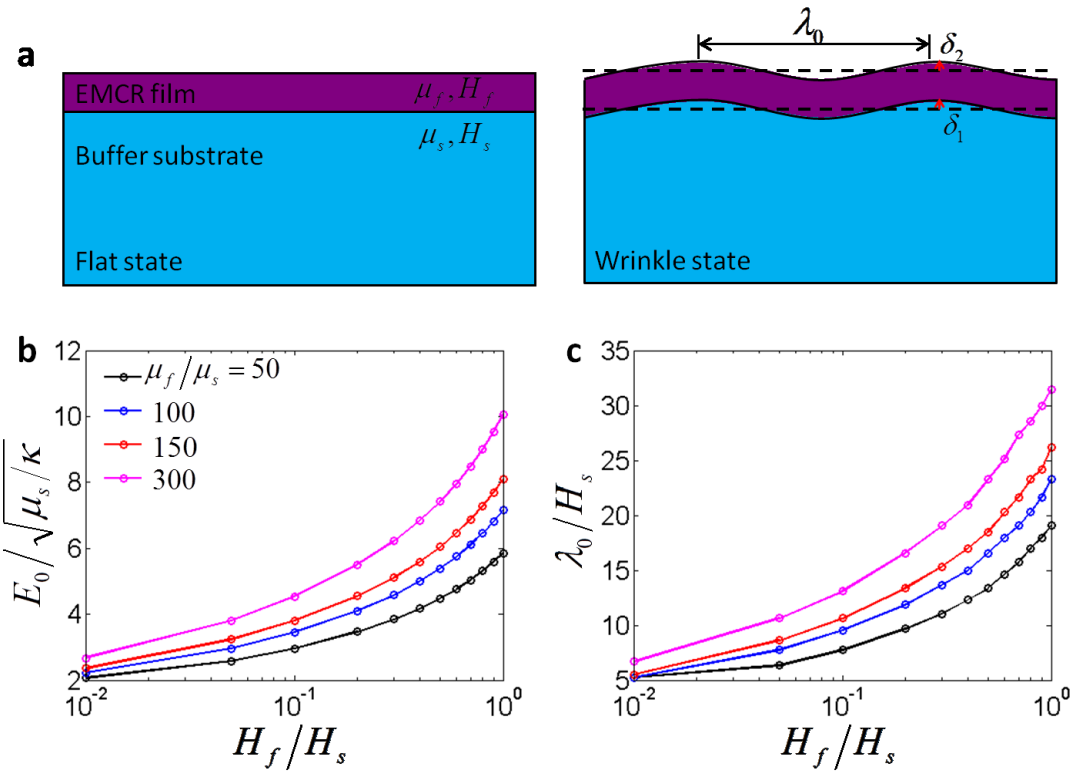

Supplementary Figure 5 | Linear stability analysis of the electro-wrinkling instability. (a) Schematic illustrations of the flat and wrinkled states. (b) The critical electric field and (c) the wavelength of the wrinkling instability as functions of film-substrate thickness ratio H_f/H_s and modulus ratio μ_f/μ_s.

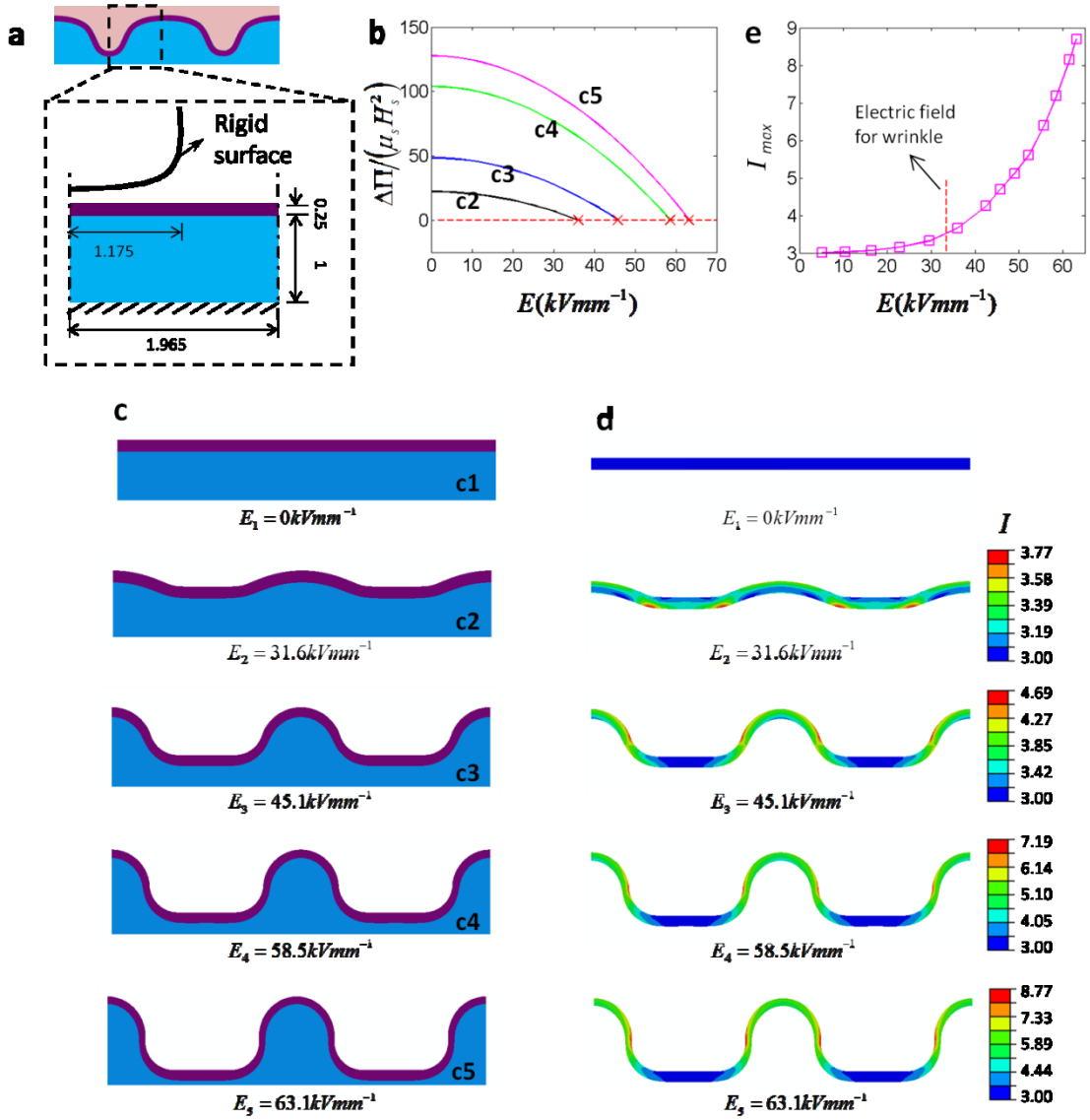

Supplementary Figure 6 | Finite-element calculations of the electro-cratering instability. (a) A 2D plane-strain model for the finite-element calculations of the electro-cratering instability. (b) The Gibbs free energy differences between cratered and flat states as functions of the applied electric field. When the Gibbs free energy difference is equal to zero, the corresponding electric fields marked by the red crosses 'x' are the electric fields in the EMCR film at the corresponding cratered states. (c) Simulated geometry and (d) the first invariant of the cratered states of the EMCR film under various electric fields. (e) The maximum first invariant in the EMCR film as a

function of the electric field. The red dash line denotes the critical electric field of the wrinkling instability calculated from **Supplementary Figure 5**.

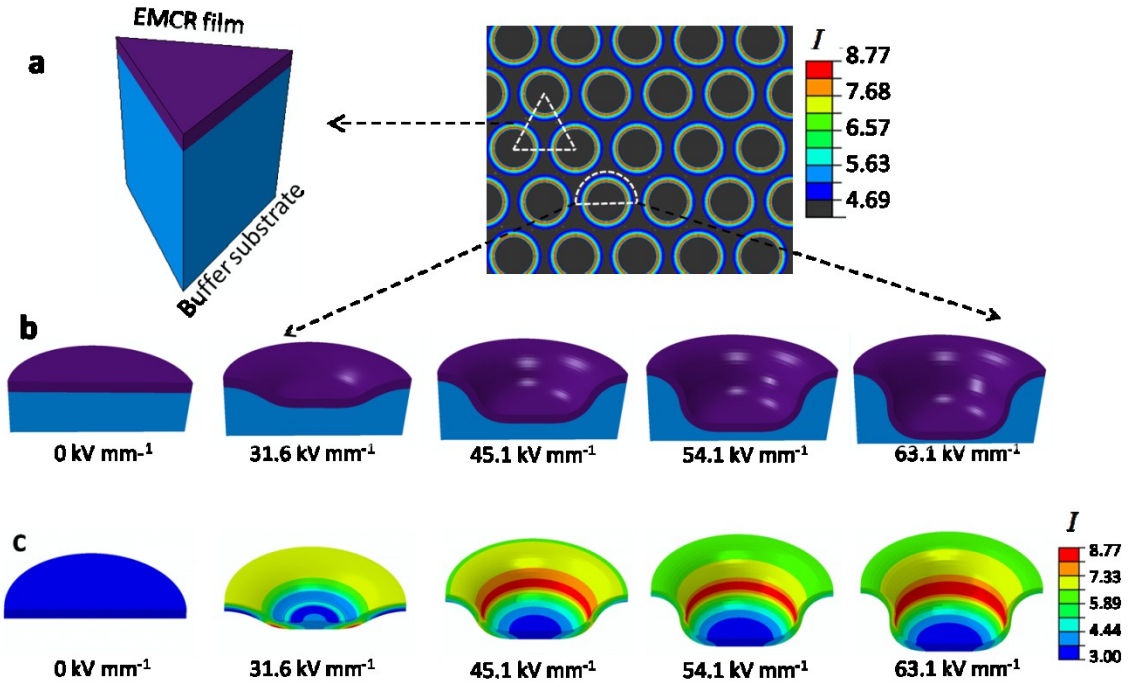

Supplementary Figure 7 | Finite-element calculations of hexagonally-distributed craters. (a) A 3D prism model for the finite-element calculations for hexagonally-distributed craters. (b) Simulated geometry and (c) the first invariant of the cratered states of the EMCR film under various electric fields.

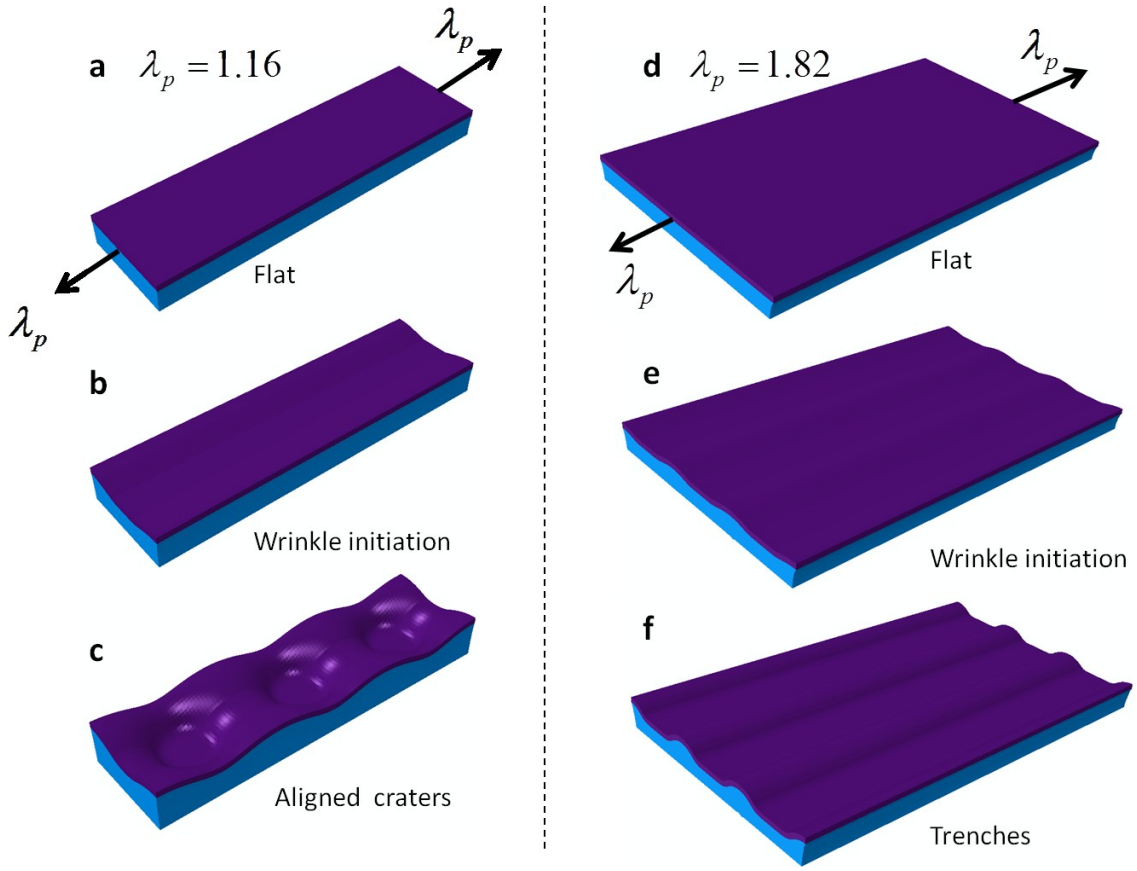

Supplementary Figure 8 | Topographical evolution of electrically-induced aligned craters and trenches. (a) A EMCR film under pre-stretch $\lambda_p = 1.16$ bonded on a buffer substrate. Simulated geometries for electrically-induced (b) aligned wrinkles and (c) aligned craters. (d) A EMCR film under pre-stretch $\lambda_p = 1.82$ bonded on a buffer substrate. Simulated geometries for electrically-induced (e) aligned wrinkles and (f) trenches.

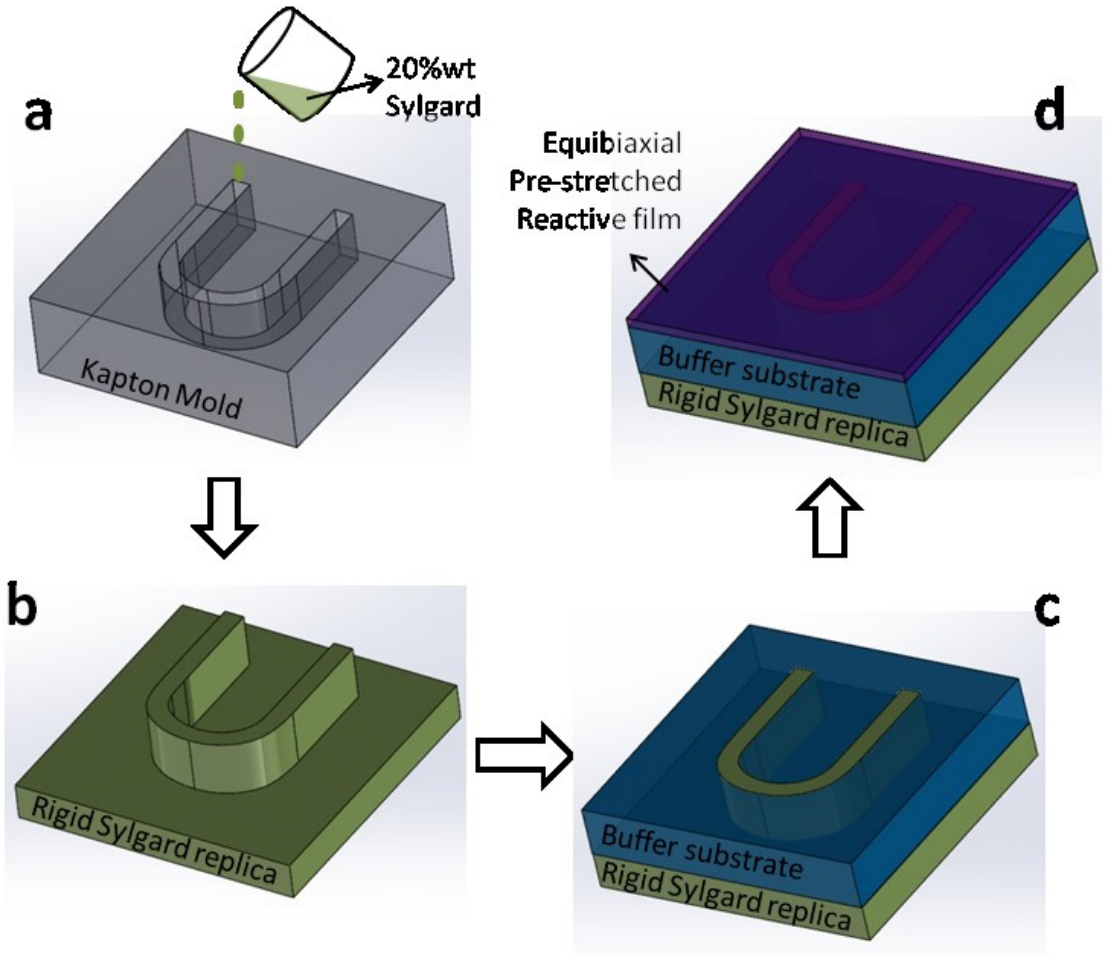

Supplementary Figure 9 | Fabrication process of the elastomer laminate for electrically-induced letter pattern. (a) A concaved letter "U" is ablated on a Kapton film (250 μm) by a laser ablation tool (Resonetics, USA). The depth of the letter is ~100 μm. A Sylgard solution (base to curing agent ratio of 5:1 by weight) is cast on the concaved letter "U" and is cured in an oven at 65^{o}C for 12 hours. The modulus of this Sylgard elastomer is around 2 MPa (15 times of the modulus of the EMCR film, and 150 times of the modulus of the buffer substrate). (b) The cured Sylgard is peeled off, and (c) a soft buffer substrate (base to curing agent 125:2 by weight) is then cast to embed the "U" object in the buffer substrate. (d) An equibaixially pre-stretched EMCR film ($\lambda_p = 0.5$) is subsequently bonded on the buffer substrate.

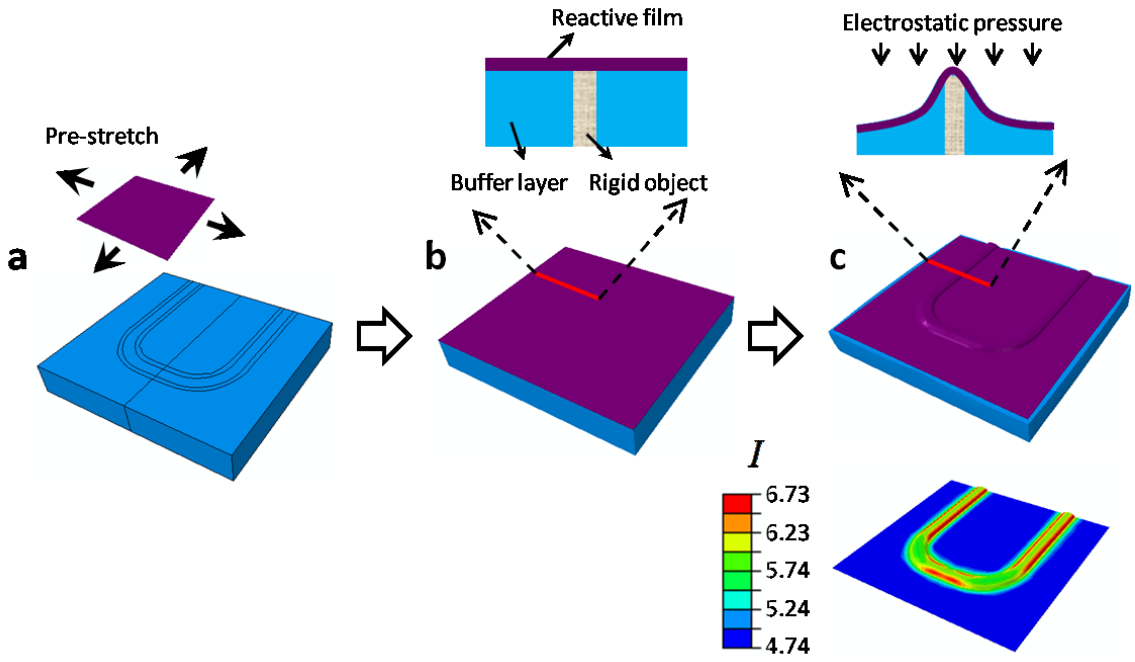

Supplementary Figure 10 | Finite-element calculations for electrically-induced pattern of letter "U". (a) A EMCR film is first equibaixially pre-stretched by $\lambda_p = 0.5$, and (b) then bonded on a buffer substrate embedded with a rigid object. (c) Simulated geometry and first invariant in the EMCR film that displays a letter "U".

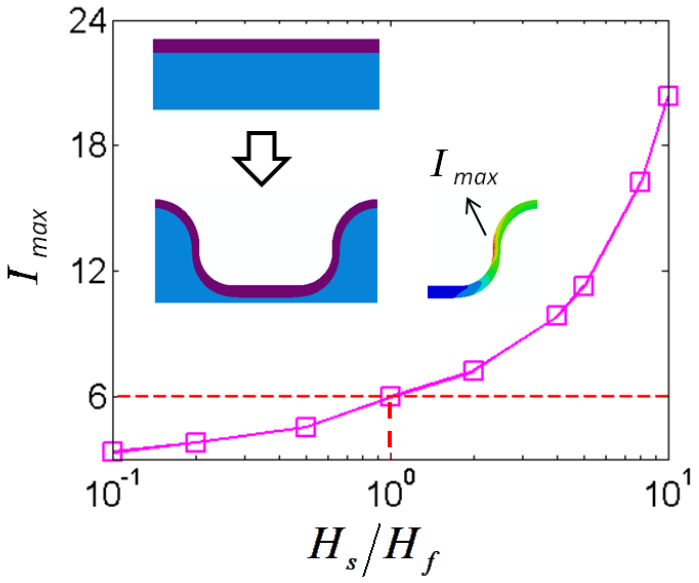

Supplementary Figure 11 | The maximum first invariant I_{max} in the EMCR film by extremely deforming the film-substrate bilayer to deepest craters as a function of substrate-film thickness ratio. According to **Fig. 1g**, the EMCR elastomer emits significant fluorescence (fluorescence intensity ratio $S/S_0>1$) only when the first invariant I is larger than 6 (denoted as the red dash line); therefore, only $H_s/H_f \geq 1$ can induce significant fluorescence emission of the EMCR elastomer.

Supplementary Methods

Linear stability analysis of the electro-wrinkling instability

An elastomer bilayer composed of an EMCR film and a buffer substrate is illustrated in **Supplementary Fig. 5a**. For simplicity, the protective insulator is not included in the current analysis. A voltage Φ is applied upon the elastomer bilayer. We denote the modulus, thickness, permittivity and applied electric field of the EMCR film as μ_f, H_f, κ_f and E_f, respectively; and the corresponding quantities of the buffer substrate as μ_s, H_s, κ_s and E_s, respectively. At the wrinkled state, the upper surface of the buffer substrate has a deflection δ_1 ($\delta_1 << H_s$), and the upper surface of the EMCR film has a deflection δ_2 ($\delta_2 << H_f$). The electric field in the elastomer bilayer follows

$$\kappa_s E_s = \kappa_f E_f \tag{1}$$

$$E_s\left(h_s + \delta_1\right) + E_f\left(h_f + \delta_2\right) = \Phi \tag{2}$$

Therefore, the electric fields can be calculated as

$$E_f = \frac{\Phi}{\left(h_f + \delta_2\right) + \frac{\kappa_f}{\kappa_s}\left(h_s + \delta_1\right)} \tag{3}$$

$$E_s = \frac{\Phi}{\frac{\kappa_s}{\kappa_f}\left(h_f + \delta_2\right) + \left(h_s + \delta_1\right)} \tag{4}$$

Since $\delta_1 / H_s << 1$ and $\delta_2 / H_f << 1$, $\kappa_f E_f^2 / 2$ and $\kappa_s E_s^2 / 2$ can be approximated as[1]

$$\frac{1}{2}\kappa_f E_f^2 \approx \frac{\kappa_f}{2}\left[\frac{\Phi^2}{\left(h_f+\frac{\kappa_f}{\kappa_s}h_s\right)^2}-\frac{2\Phi^2}{\left(h_f+\frac{\kappa_f}{\kappa_s}h_s\right)^3}\frac{\kappa_f}{\kappa_s}\delta_1-\frac{2\Phi^2}{\left(h_f+\frac{\kappa_f}{\kappa_s}h_s\right)^3}\delta_2\right] \quad (5)$$

$$\frac{1}{2}\kappa_s E_s^2 \approx \frac{\kappa_s}{2}\left[\frac{\Phi^2}{\left(\frac{\kappa_s}{\kappa_f}h_f+h_s\right)^2}-\frac{2\Phi^2}{\left(\frac{\kappa_s}{\kappa_f}h_f+h_s\right)^3}\delta_1-\frac{2\Phi^2}{\left(\frac{\kappa_s}{\kappa_f}h_f+h_s\right)^3}\frac{\kappa_s}{\kappa_f}\delta_2\right] \quad (6)$$

Mechanical equilibrium condition in the EMCR film can be expressed as

$$\mu_f \nabla^2 \mathbf{u}_f - \nabla P_f = 0 \quad (7)$$

Where $\mathbf{u}_f = \begin{bmatrix} u_{fx} & u_{fy} \end{bmatrix}^T$ is the displacement vector in the EMCR elastomer, and P_f is the hydrostatic pressure that enforces the incompressibility of the elastomers. The stress in the EMCR elastomer follows

$$\boldsymbol{\sigma}_f = \boldsymbol{\sigma}_{mf} + \boldsymbol{\sigma}_{ef} \quad (8)$$

$$\boldsymbol{\sigma}_{mf} = \begin{bmatrix} 2\mu_f u_{fx,x} - P_f & \mu_f\left(u_{fx,y}+u_{fy,x}\right) \\ \mu_f\left(u_{fx,y}+u_{fy,x}\right) & 2\mu_f u_{fy,y} - P_f \end{bmatrix} \quad (9)$$

$$\boldsymbol{\sigma}_{ef} = \varepsilon_f \mathbf{E}_f \otimes \mathbf{E}_f - \frac{1}{2}\varepsilon_f \left|\mathbf{E}_f\right|^2 \mathbf{I} = \begin{bmatrix} -\frac{1}{2}\varepsilon_f E_f^2 & 0 \\ 0 & \frac{1}{2}\varepsilon_f E_f^2 \end{bmatrix} \quad (10)$$

where $\boldsymbol{\sigma}_{mf}$ and $\boldsymbol{\sigma}_{ef}$ are mechanical stress tensor and electric-field-induced stress tensor in the EMCR film; $u_{fx,y}$ represent the y -direction gradient of the x -direction displacement component of $\mathbf{u}_f$; and $\mathbf{E}_f = \begin{bmatrix} 0 & E_f \end{bmatrix}^T$ is the electric field vector in the elastomer.

To solve the problem, we first consider the incompressibility of the elastomer, which can be expressed as

$$\nabla \cdot \mathbf{u}_f = 0 \tag{11}$$

Based on **Supplementary Eq. (11)**, a stream function Θ_f can be used to express the displacement as

$$\begin{cases} u_{fx} = \dfrac{\partial \Theta_f}{\partial y} \\ u_{fy} = -\dfrac{\partial \Theta_f}{\partial x} \end{cases} \tag{12}$$

We perturb the solution of Θ_f and P_f as

$$\begin{cases} \Theta_f(x,y) = \varphi_f(y)\cos(kx) \\ P_f(x,y) = p_f(y)\sin(kx) \end{cases} \tag{13}$$

From **Supplementary Eq. (7)**, we obtain

$$\begin{cases} \mu_f\left(-k^2\dfrac{d\varphi_f}{dy} + \dfrac{d^3\varphi_f}{dy^3}\right) - kp_f = 0 \\ \mu_f\left(-k^3\varphi_f + k\dfrac{d^2\varphi_f}{dy^2}\right) - \dfrac{dp_f}{dy} = 0 \end{cases} \tag{14}$$

The general solutions for **Supplementary Eq. (14)** are

$$\varphi_f(y)=\frac{1}{4}e^{-ky}\left(2+2e^{2ky}+ky-e^{2ky}ky\right)c_{f1}+\frac{e^{-ky}\left(-1+e^{2ky}\right)}{2k}c_{f2}+\frac{e^{-ky}\left(-1+e^{2ky}\right)y}{4k}c_{f3}+\frac{e^{-ky}\left(1-e^{2ky}+ky+e^{2ky}ky\right)}{4k^2\mu_f}c_{f4} \quad (15)$$

$$p_f(y)=\frac{1}{2}e^{-ky}\left(1-e^{2ky}\right)k^2\mu_f c_{f1}+\frac{1}{2}e^{-ky}\left(-1+e^{2ky}\right)\mu_f c_{f3}+\frac{1}{2}e^{-ky}\left(1+e^{2ky}\right)c_{f4} \quad (16)$$

A similar analysis of the buffer substrate can give the corresponding φ_s and p_s for the substrate as

$$\varphi_s(y)=\frac{1}{4}e^{-ky}\left(2+2e^{2ky}+ky-e^{2ky}ky\right)c_{s1}+\frac{e^{-ky}\left(-1+e^{2ky}\right)}{2k}c_{s2}+\frac{e^{-ky}\left(-1+e^{2ky}\right)y}{4k}c_{s3}+\frac{e^{-ky}\left(1-e^{2ky}+ky+e^{2ky}ky\right)}{4k^2\mu_s}c_{s4} \quad (17)$$

$$p_s(y)=\frac{1}{2}e^{-ky}\left(1-e^{2ky}\right)k^2\mu_s c_{s1}+\frac{1}{2}e^{-ky}\left(-1+e^{2ky}\right)\mu_s c_{s3}+\frac{1}{2}e^{-ky}\left(1+e^{2ky}\right)c_{s4} \quad (18)$$

There are eight unknown variables c_{si} and c_{fi} in **Supplementary Eqs. (15-18)**, where *i*=1-4. The unknown variables can be solved with the following boundary conditions.

An *y=0*, the bottom surface of the substrate , the displacement of the buffer substrate is fixed and can be expressed as

$$\mathbf{u}_s=\mathbf{0}, \quad \text{on } y=0 \quad (19)$$

At $y=h_s$, the top surface of the substrate, the force and displacement in elastomer bilayer should be continuous, thus

$$\begin{cases} \mathbf{n}_x \cdot \boldsymbol{\sigma}_s \cdot \mathbf{n}_y = \mathbf{n}_x \cdot \boldsymbol{\sigma}_f \cdot \mathbf{n}_y \\ \mathbf{n}_y \cdot \boldsymbol{\sigma}_s \cdot \mathbf{n}_y = \mathbf{n}_y \cdot \boldsymbol{\sigma}_f \cdot \mathbf{n}_y \\ \mathbf{u}_s = \mathbf{u}_f \end{cases}, \quad \text{on } y=h_s \tag{20}$$

where $\mathbf{n}_x = \begin{bmatrix} 1 & 0 \end{bmatrix}^T$ denotes the unit vector in x direction, and $\mathbf{n}_y = \begin{bmatrix} 0 & 1 \end{bmatrix}^T$ denotes the unit vector in y direction.

At $y=h_s+h_f$, the top surface of the EMCR film, the surface tractions should be 0, thus

$$\begin{cases} \mathbf{n}_x \cdot \boldsymbol{\sigma}_f \cdot \mathbf{n}_y = 0 \\ \mathbf{n}_y \cdot \boldsymbol{\sigma}_f \cdot \mathbf{n}_y = 0 \end{cases}, \quad \text{on } y=h_s+h_f \tag{21}$$

The above boundary conditions, **Supplementary Eqs. (19-21)**, can be re-written as

$$\begin{cases} u_{sx} = 0 \\ u_{sy} = 0 \end{cases}, \text{ On } y=0 \tag{22}$$

$$\begin{cases} \sigma_{sexy} = \sigma_{fexy} \\ \sigma_{seyy} - \dfrac{\kappa_s \Phi^2}{\left(\dfrac{\kappa_s}{\kappa_f} h_f + h_s \right)^3} \left(\delta_1 + \dfrac{\kappa_s}{\kappa_f} \delta_2 \right) = \sigma_{feyy} - \dfrac{\kappa_f \Phi^2}{\left(h_f + \dfrac{\kappa_f}{\kappa_s} h_s \right)^3} \left(\dfrac{\kappa_f}{\kappa_s} \delta_1 + \delta_2 \right) \\ u_{sx} = u_{fx} \\ u_{sy} = u_{fy} \end{cases}, \text{ on } y=h_s \tag{23}$$

$$\begin{cases} \sigma_{fexy} = 0 \\ \sigma_{feyy} - \dfrac{\kappa_f \Phi^2}{\left(h_f + \dfrac{\kappa_f}{\kappa_s} h_s \right)^3} \left(\dfrac{\kappa_f}{\kappa_s} \delta_1 + \delta_2 \right) = , \end{cases} \text{ on } y=h_s+h_f \tag{24}$$

Supplementary Eqs. (22-24) can be further expressed as functions of φ_f, p_f, φ_s and p_s

$$\begin{cases} \varphi_s = 0 \\ \dfrac{d\varphi_s}{dy} = 0 \end{cases}, \quad \text{on } y=0 \tag{25}$$

$$\begin{cases} \dfrac{d^2\varphi_s}{dy^2} + k\varphi_s = \dfrac{d^2\varphi_f}{dy^2} + k\varphi_f \\ 2\mu_s k\dfrac{d\varphi_s}{dy} - Yk\left(\varphi_s + \varphi_f\right) - p_s = 2\mu_f k\dfrac{d\varphi_f}{dy} - Yk\left(\varphi_f + \varphi_s\right) - p_f \\ \dfrac{d\varphi_s}{dy} = \dfrac{d\varphi_f}{dy} \\ \varphi_s = \varphi_f \end{cases}, \text{ on } y=h_s \tag{26}$$

where $Y = \dfrac{\kappa\Phi^2}{\left(h_f + h_s\right)^3} = \dfrac{\kappa E^2}{\left(h_f + h_s\right)}$ and $\kappa_f = \kappa_s = \kappa$.

$$\begin{cases} \dfrac{d^2\varphi_f}{dy^2} + k\varphi_f = 0 \\ 2\mu_f k\dfrac{d\varphi_f}{dy} - Yk\left(\varphi_f + \varphi_s\right) - p_f = 0 \end{cases}, \text{ on } y=h_s+h_f \tag{27}$$

Substituting **Supplementary Eqs. (15-18)** in to **Supplementary Eqs. (25-27)**, we obtain

$$\mathbf{D} \cdot \begin{bmatrix} c_{s1} \\ c_{s2} \\ c_{s3} \\ c_{s4} \\ c_{f1} \\ c_{f2} \\ c_{f3} \\ c_{f4} \end{bmatrix} = 0 \tag{28}$$

The existence of roots requires the determinant of the coefficient matrix $\mathbf{D}$ in **Supplementary Eq. (28)** to be zero, i.e. $\det(\mathbf{D}) = 0$. The corresponding electric field E_0 and critical wavelength

$\lambda_0 = 2\pi/k$ have been calculated in **Supplementary Fig. 5b**. For the device illustrated in **Fig. 3**, the calculated critical electric field for wrinkling instability is E_0=33.5 kV mm^{-1}, very close to the experimentally observed value 27-32 kV mm^{-1}.

Finite-element analysis of the electro-cratering instability

We compute the electric fields for formation of craters by comparing the Gibbs free energy between the cratered and flat states. The Gibbs free energy difference is

$$\Delta\Pi = \Pi_{Crater} - \Pi_{Flat} \tag{29}$$

where Π_{Crater} and Π_{Flat} are the Gibbs free energy for cratered and flat states, respectively. At the flat state, since the elastic energy is zero and the electric field through the elastomer laminate is uniform, the Gibbs free energy can be expressed as

$$\Pi_{Flat} = -\frac{\kappa E^2}{2}\left(H_f + H_s\right)A \tag{30}$$

where A is the surface area of analysis domain. For the cratered state, we calculate the Gibbs free energy using a commercial finite element software, ABAQUS6.10.1. To approximate the cratered geometry (i.e. wavelength and diameter in **Fig. 4c**), we first compress the elastomer bilayer with a rigid surface to different depths as shown in **Supplementary Fig. 6**. Subsequently, we calculate the elastic energy and electrostatic potential energy of the elastomer bilayer based on the cratered geometry[1-3]. The Gibbs free energy difference decreases with the applied electric field (**Supplementary Fig. 6b**). When the Gibbs free energy difference is equal to zero, the corresponding electric fields are the electric fields in the EMCR film at the cratered states. The corresponding electric fields are marked by the red crosses 'x' in **Supplementary Fig. 6b**.

Supplementary References

1. Wang Q, Zhao X. Creasing-wrinkling transition in elastomer films under electric fields. *Physical Review E* **88**, 042403 (2013).

2. Wang Q, Tahir M, Zhang L, Zhao X. Electro-creasing instability in deformed polymers: experiment and theory. *Soft Matter* **7**, 6583-6589 (2011).

3. Wang Q, Suo Z, Zhao X. Bursting drops in solid dielectrics caused by high voltages. *Nature Communications* **3**, 1157 (2012).